Riset Geologi dan Pertambangan
(Geology and Mining Research)

RESEARCH ARTICLE

OPEN ACCESS

Riset Geologi dan Pertambangan (2025) Vol. 35, No. 2, 73–88
DOI: 10.55981/risetgeotam.2025.1379

Keywords:
Geoelectrical resistivity
Dipole-dipole configuration
Cone Penetration Test
Liquefaction

Corresponding author:
Adi Susilo
adisusilo@ub.ac.id

Article history:
Received: 17 April 2025
Revised: 15 May 2025
Accepted: 08 July 2025

Author Contributions:
Conceptualization: VV, AS
Data curation: VV
Formal analysis: VV
Funding acquisition: SAINTEK, UB STARS
Investigation: VV
Methodology: VV, AS, WOS
Supervision: AS, WOS
Visualization: VV, AS, WOS
Writing – original draft: VV
Writing – review & editing: VV, AS, WOS

Citation:
Volvacea, V., Susilo, A., Sumartini, W., O., 2025. Evaluation of liquefaction potential according to resistivity and CPT Data. *Riset Geologi dan Pertambangan, 35 (2)*, 73–88, doi: 10.55981/risetgeotam.2025.1379

Evaluation of Liquefaction Potential According to Resistivity and CPT Data

Volvariella Volvacea[1], Adi Susilo[2], Wa Ode Sumartini[3]

[1]Physics Department, Universitas Brawijaya, Malang, Indonesia
[2]Research Center for Geological Disaster, BRIN, Bandung, Indonesia
[3]Central Study of Geoscience and Hazard Mitigation, Universitas Brawijaya, Malang, Indonesia

Abstract

This study investigates the liquefaction potential in Tambak Wedi Subdistrict, Surabaya, employing the electrical resistivity geophysical method with a dipole-dipole configuration and the Cone Penetration Test (CPT). The electrical resistivity method is utilized to accees the resistivity values of soil layers and to generate a 2D subsurface profile. The CPT method is applied to confirm the soil layer types and to compute the safety factor (SF). The soil data from both methods are subsequently analyzed to evaluate the liquefaction potential based on the soil resistivity and SF values. The analysis incorporates a Peak Ground Acceleration (PGA) of 0.3g and considers an earthquake magnitude of 7.5 Mw. The findings from this study reveal that the soil layers ranging from sandy to organic soil, with dominant silt-sandy and clay-silt layers present up to a depth of 10 meters, and clay-silt and clay layers from 11 to 20 meters. Except in the first 2 meters depth, the calculated SF is less than 0.6, indicating a high liquefaction potential in the region. The assessment of liquefaction potential in this study involved the calculation of N-SPT, Liquefaction Potential Index (LPI), and Liquefaction Severity Index (LSI). These findings underscore the importance of incorporating site-specific geotechnical evaluations into disaster risk reduction strategies, as they provide critical input for the development of effective mitigation plans aimed at minimizing potential loss of life and economic impact.

1. Introduction

Liquefaction is a phenomenon resulting from the transformation of solid sediments into a liquid state, induced by cyclic shear stresses during an earthquake event (Hardy et al., 2015). This occurrence typically arises when the soil is water-saturated and fine-grained, limiting its capacity to absorb water efficiently, consequently causing an increase in pore water pressure. An area is deemed susceptible to liquefaction (Seed and Idriss, 1971) if the soil exhibits non-cohesive characteristics, uniform grain size distribution, composed primarily of fine sand, which leads to the generation of pore water pressure, a low soil density rasio, and the formation of loose sandy layers. Furthermore, younger soil deposits, such as Holocene layers, and prolonged ground shaking during seismic activity, are contributing factors to liquefaction potential.

During large-scale earthquakes, the pore water pressure is subjected to intense shaking, potentially exceeding the frictional strength of the soil. This results in a sudden rise in pore water pressure, leading to the possibility of liquefaction at the surface. Areas prone to liquefaction are typically composed of Quaternary deposits, including water-saturated sand-gravel and silt-sand layers, with a shallow groundwater table (Hardy et al., 2015).

The objective of this study is to assess the liquefaction potential in Surabaya, a rapidly growing city. Surabaya's soil consists of alluvial types, which are derived from riverine deposits with relatively young soil ages. Coastal areas, particularly those designated for residential settlements, fisheries, ponds, warehouses, military, shipbuilding industries, ports, and coastal tourism, are found in the vicinity of the Suramadu Bridge (Surabaya, 2016). The study utilizes the previously established Peak Ground Acceleration (PGA) values, as researched by the Indonesian Earthquake Map Revision Team, employing the total probability method with a three-dimensional earthquake source model. The results indicate that the PGA in the study area ranges from 0.3 to 0.4 g (Irsyam et al., 2010).

2. Geologic setting

According to the geological map, the subsurface composition of Surabaya comprises alluvial deposits, sandstone units, and several distinct geological formations, namely the Kabuh, Pucangan, Lidah, and Sonde Formations. These formations are characterized by the presence of interbedded sandstone and clay layers, indicating a complex sedimentary environment. This study was conducted in the Tambak Wedi Subdistrict of Surabaya, an area characterized by alluvial soil deposits originating from fluvial sedimentation comprising sandstone and clay as depicted in Figure 1. Coastal deposits in this region exhibit a high susceptibility to liquefaction, particularly when associated with geologically young strata (Green and Ziotopoulou, 2015). Based on these findings, it is inferred that the soil layers across Surabaya generally possess a uniform potential for liquefaction.

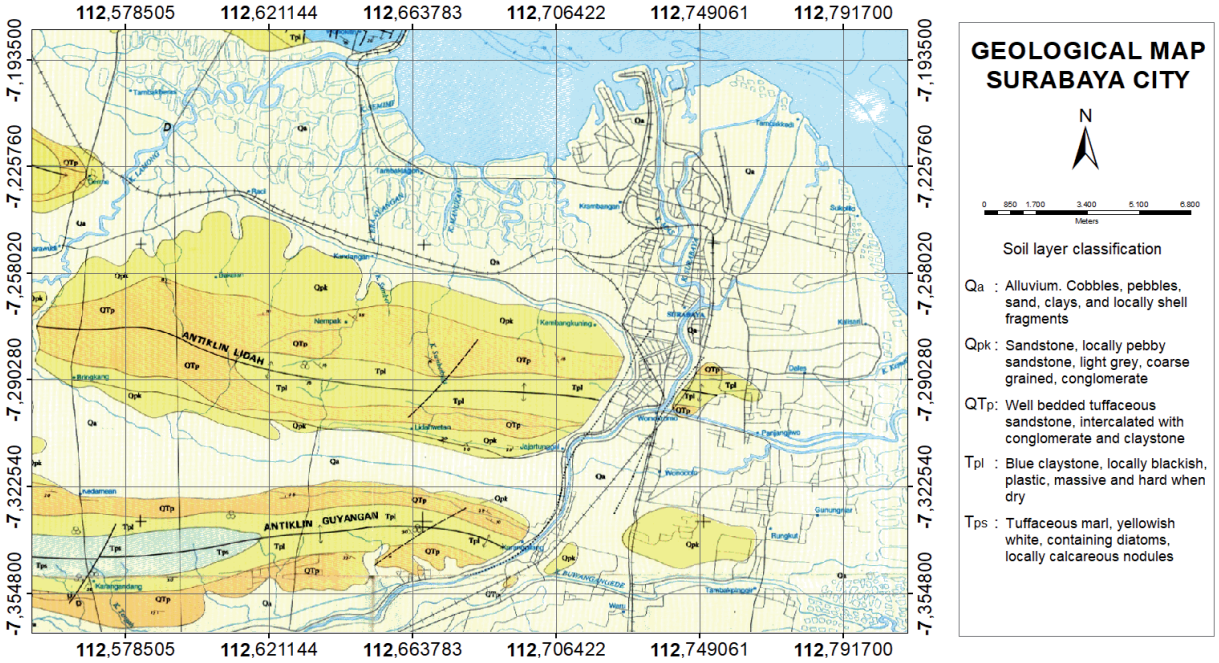

Figure 1 The geological map and coordinates of Surabaya City.

The liquefaction potential study was conducted from October 12–14, 2024. Three sampling points were selected, considering the challenges posed by the terrain. At each site, measurements were taken using three geoelectric traverses and two CPT points, as depicted in Figures 2.

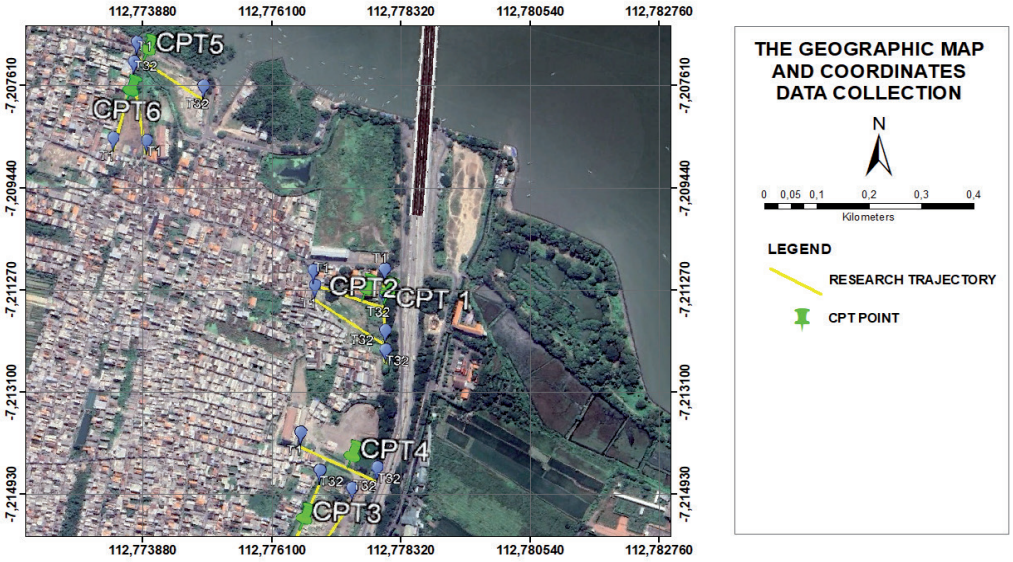

Figure 2 The geological map and coordinates of of the data collection site in Surabaya City.

3. Data and methods

This study utilizes two primary datasets, electrical resistivity and cone tip resistance (q_c). Electrical resistivity measurements were acquired using geoelectrical surveying techniques to characterize subsurface soil types, determine resistivity values, and identify the groundwater table. q_c data were obtained through Cone Penetration Testing (CPT), providing insights into soil classification and Strength Factor (SF) values. Both datasets were systematically analyzed to evaluate the correlation between soil resistivity and SF, which serves as the basis for determining Liquefaction Susceptibility Index (LSI) and Liquefaction Potential Index (LPI).

Resistivity method

Geoelectricity method is employed to assess the electrical properties of the Earth by injecting high-voltage electrical current into the subsurface through two electrodes (Telford et al., 1928). As the separation between the current electrodes increases, the current can penetrate deeper into the rock layers. The presence of an electrical current flow induces a corresponding electrical potential in the ground, which is then measured using a voltmeter connected through two additional electrodes, positioned at a shorter distance than the current electrodes. This results in the calculation of apparent resistivity, which can be expressed mathematically

$$\rho_a = k\frac{V}{I} \tag{1}$$

where k is the geometric factor and ρ_a is the value of the apparent resistivity.

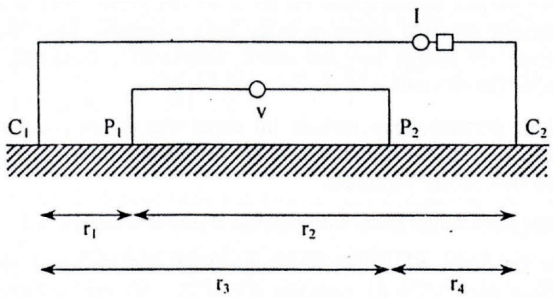

Figure 3 illustrates the standard configuration of a four-electrode system used in resistivity measurements, comprising a pair of current electrodes (C_1, C_2) and a pair of potential electrodes (P_1, P_2).

Electrodes C_1 and C_2 serve as current sources, while electrodes P_1 and P_2 are utilized for measuring the potential difference. The electrical current is introduced into the ground through electrodes C_1 and C_2, and the potential difference is subsequently recorded using a voltmeter connected to electrodes P_1 and P_2, as illustrated in Figure 5. It can be described by the equation

$$\Delta V = VP_1 - VP_2 = \frac{I\rho}{2\pi}\left\{\left(\frac{1}{r_1}-\frac{1}{r_2}\right)-\left(\frac{1}{r_3}-\frac{1}{r_4}\right)\right\} \quad (2)$$

Based on the equation above, the apparent resistivity of the medium can be determined using the following formula

$$\rho_a = \frac{\Delta V}{I}\frac{2\pi}{\left\{\left(\frac{1}{r_1}-\frac{1}{r_2}\right)-\left(\frac{1}{r_3}-\frac{1}{r_4}\right)\right\}} \quad (3)$$

The value of the geometric factor, *k*, is determined

$$k = \frac{2\pi}{\left\{\left(\frac{1}{r_1}-\frac{1}{r_2}\right)-\left(\frac{1}{r_3}-\frac{1}{r_4}\right)\right\}} \quad (4)$$

Data acquisition using the resistivity geoelectric method was conducted by deploying a 160-meter-long cable, with electrodes positioned at 10-meter intervals. In contrast, for the CPT method, measurement points were located along the geoelectric line, with a minimum spacing of 50 meters between each sampling point, and a consistent depth of 20 meters for each measurement.

For the configuration in this research is using the dipole-dipole configuration. The distance between the current electrode and the potential electrode is denoted by *a*, while the separation between the midpoints of the electrodes is *L*, as illustrated in Figure 5. It is essential that *L* exceeds a, as indicated by Lowrie (2007).

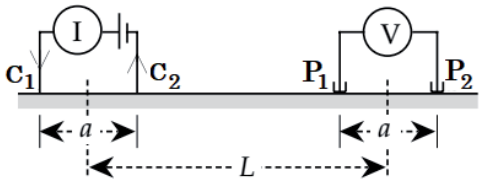

Figure 4 Dipole-dipole configuration in geoelectric resistivity method.

Thus, the apparent resistivity value in the dipole-dipole configuration can be calculated using the equation

$$\rho_a = \pi\frac{V}{I}\frac{L(L^2-a^2)}{a^2} \quad (5)$$

Thus, the geometric factor *k* value in the dipole-dipole configuration is obtained as

$$k = \pi(n+2)(n+1)\,n.r \quad (6)$$

The acquired data is subsequently processed using the Res2Dinv software to produce a 2D model of the subsurface layers. From this 2D representation, the resistivity values for aech layer at various depths are determined. The soil resistivity values will be used to determine the soil classification type using Table 1.

Table 1 The soil resistivity values of several soil type

Soil Type	Resistivity (Ωm)
Clay	1 – 100
Alluvium	1 – 1000
Gravel	100 – 10,000
Sandstone	1 – 1000

CPT Method

The Cone Penetration Test (CPT) is a widely employed technique for soil investigation aimed at determining the geotechnical properties of soil at specific sites. This method involves the insertion of a cone probe, which is equipped with sensors to measure shear resistance and hydraulic pressure, into the ground at a constant rate of penetration. In the context of cone penetration testing, the obtained data typically include tip resistance (q_c) and sleeve friction (f_s) values. These parameters are used to calculate the friction ratio (FR), which is instrumental in classifying the soil type according to the Robertson classification system (Robertson, 2010).

$$F_R = \frac{f_s}{q_c} 100\% \tag{7}$$

Soils with finer grain textures (silt-clay), the q_c tends to be low, whereas the friction ratio (FR) increases. Conversely, in soils with coarser grain textures (sand-gravel), q_c values are higher, while FR values decrease (Ambarwati et al., 2020). Subsequent data analysis for assessing liquefaction potential involves calculating the safety factor (SF) using the equation provided.

$$SF = \frac{CRR}{CSR} MSF \tag{8}$$

where CRR represents the cyclic resistance ratio, CSR denotes the cyclic stress ratio, and MSF is the earthquake magnitude scaling factor. The CSR value can be determined using the equation proposed by Seed and Idriss (1971), as outlined below.

$$CSR = 0{,}65 \frac{a_{max}}{g} . \frac{\sigma_{vo}}{\sigma'_{vo}} . r_d \tag{9}$$

In this context, a_{max} represents the maximum gravitational acceleration at the peak, g denotes the gravitational acceleration of the Earth (9.8 m/s^2), σ_{vo} refers to the total vertical stress (in kPa), σ'_{vo} is the effective vertical stress (in kPa), and r_d is the stress reduction coefficient, which varies with depth z.

The value of r_d is determined as a function of the depth beneath the ground surface, with the criteria,

if the depth $z \leq 9.15$ m, then
$$r_d = 1{,}0 - 0{,}00765\, z$$
if the depth between $9.15 \leq z < 23$ m, then
$$r_d = 1{,}174 - 0{,}0267\, z$$
if the depth between $23 \text{ m} \leq z < 30$ m, then
$$r_d = 0{,}744 - 0{,}0008\, z$$
if the depth $z \geq 9.15$ m, then
$$r_d = 0{,}5$$
(10)

Liquefaction Risk Factors

The potential occurrence of soil liquefaction is influenced by various factors, including soil strength commonly represented by the Standard Penetration Test (SPT) N-value and the severity of the liquefaction itself. A correlation exists between the N-SPT value and the cone penetration resistance (q_c), expressed by the relationship $n = q_c/N$, where n denotes the correlation factor (Sudjatmiko, 2022). The classification of soil strength can subsequently be derived from the N-SPT values, as outlined in Table 2 (Susilo et al., 2019).

Table 2 Correlation between N-SPT value and soil susceptibility.

N-SPT	Soil Packing
< 4	Very loose
4 – 10	Loose
10 – 30	Compact
30 – 50	Dense
> 50	Very dense

The liquefaction potential of a site can be quantitatively evaluated through the Liquefaction Potential Index (LPI), which integrates safety factor (SF) values across a depth interval of 0 to 20 meters, following the methodology established by Iwasaki et al. (1982).

$$LPI = \int_0^{20} F(z)(20 - z)\ dz \tag{11}$$

in which,

$$\begin{aligned} &F = 1 - SF \text{ for } SF \leq 1 \\ &F = 0 \text{ for } SF > 1 \\ &w(z) = 10 - 0.5z \end{aligned} \tag{12}$$

In this context, z denotes depth in meters. The outcomes derived from Equation 11 are subsequently classified to assess the extent of soil damage resulting from liquefaction, as summarized in Table 3.

Table 3 Categories based on LPI (Iwasaki et al., 1982).

LPI	Category
0	Very low
0 < LPI ≤ 5	Low
5 < LPI ≤ 15	High
15 > LPI	Very high

Furthermore, the Liquefaction Severity Index (LSI) is computed to quantify the potential intensity of liquefaction events. This index relies exclusively on the safety factor (SF) parameter and is defined by the following equation

$$LSI = \int_0^{20} P_L(z)(10 - 0.5z)\ dz \tag{13}$$

in which,

$$P_L(z) = \frac{1}{1 + \left(\frac{SF}{0.96}\right)^{4.5}} \quad \text{for SF} \leq 1.411 \tag{14}$$

$$P_L = 0 \text{ for SF} > 1.411$$

In this context, z denotes depth in meters, while $P_L(z)$ corresponds to the probability of liquefaction occurrence at the specified depth. The calculated LSI values are then classified into distinct categories based on the framework outlined in Table 4 (Sonmez, 2003).

Table 4 Categories based on LSI (Sonmez, 2003).

LSI	Category
85 ≤ LSI <100	Very high
65 ≤ LSI < 85	High
35 ≤ LSI < 65	Moderate
15 ≤ LSI < 35	Low
0 < LSI < 15	Very low
LSI = 0	Non-liquefied

4. Results

Analysis of Data Using the Resistivity Geoelectrical Method

At the first testing location, the initial survey line was oriented from northwest to southeast, spanning the coordinates 7°12'41.44" S, 112°46'36.56" E to 7°12'44.35" S, 112°46'40.90" E. Figure 5 shows the map of the first test location.

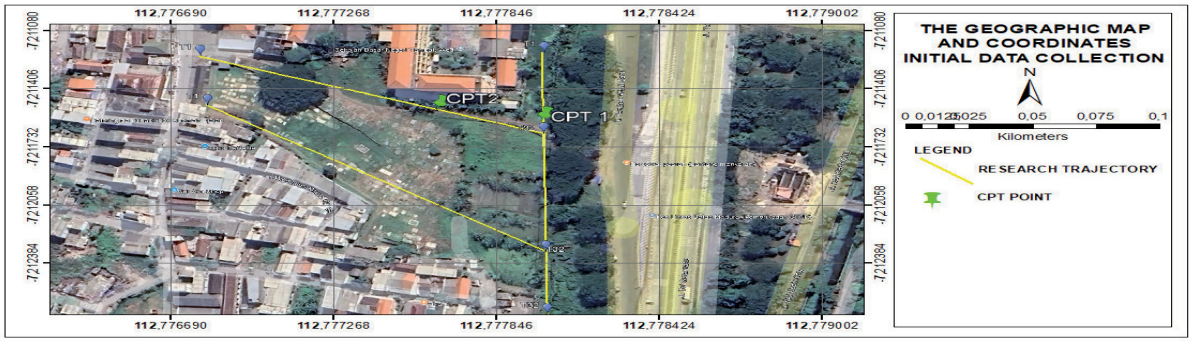

Figure 5 The geographic map and coordinates corresponding to the initial data collection site.

The groundwater table level can be determined from the interpretation of resistivity measurements which is located at the upper part of saturated layer. The resulting 2D subsurface profile, as shown in Figure 6(a), indicated a resistivity range of 0.766 Ωm to 25.3 Ωm, which was interpreted as a clay or a sandstone layer. The second survey line was oriented from west-northwest to east-southeast, spanning the coordinates 7°12'40.46" S, 112°46'36.47" E to 7°12'42.00" S, 112°46'40.87" E, as depicted in Figure 6(b). The resistivity values in this section ranged from 4.40 Ωm to over than 60.5 Ωm, also interpreted as a clay or a sandstone layer. In the third survey line, oriented from north to south and spanning the coordinates 7°12'40.40" S, 112°46'40.88" E to 7°12'45.59" S, 112°46'40.92" E (Figure 6(c)), the resistivity values ranged from 4.40 Ωm to over than 60.5 Ωm, interpretated as a clay or a sandstone layer. Based on the resistivity data obtained from the three survey lines, it can be concluded that the subsurface composition at the study site is predominantly characterized by a clay or a sandstone layer.

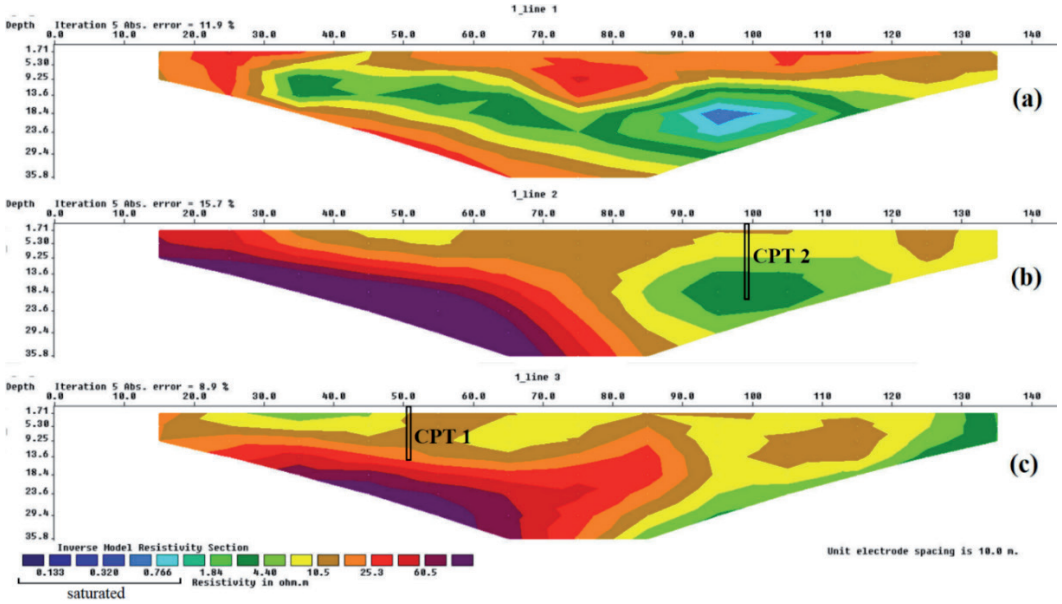

Figure 6 Two-dimensional cross-sectional representation of subsurface layers at the initial site: (a) first profile, (b) second profile, and (c) third profile.

At the second testing location, the first survey line was oriented from the southwest to the northeast, spanning the coordinates 7°12'58.09" S, 112°46'34.87" E to 7°12'53.26" S, 112°46'36.86" E. Figure 7 shows the map of the first test location.

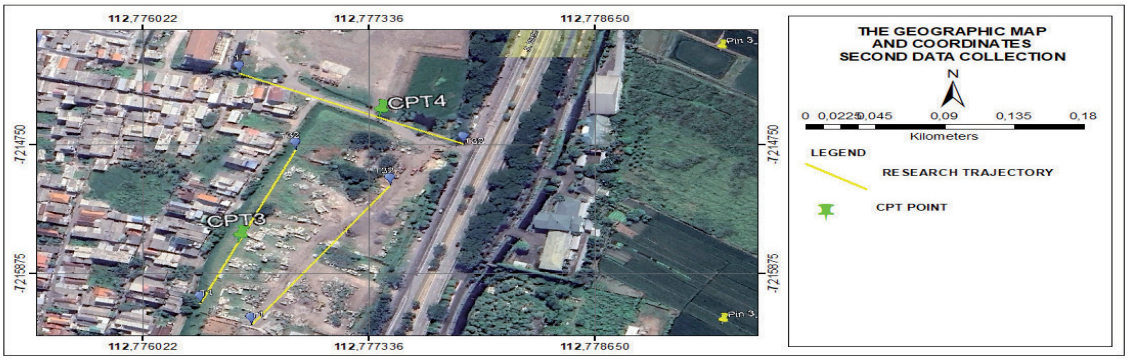

Figure 7 The geographic map and coordinates corresponding to the second data collection site.

The groundwater table level can be determined from the interpretation of resistivity measurements which is located at the upper part of saturated layer. The resulting 2D subsurface profile is illustrated in Figure 8(a). Resistivity values along this line ranged from 0.32 Ωm to 60.5 Ωm. Soil layers with resistivity values between 1 Ωm and 100 Ωm were interpreted as clay or sandstone formations. For the second survey line, the cable was positioned from the southwest to the northeast, with coordinates 7°12’58.75” S, 112°46’35.94” E to 7°12’54.37” S, 112°46’38.85” E, as shown in Figure 8(b). Resistivity values on this line varied from 0.32 Ωm to 10.5 Ωm, and the layer was similarly interpreted as clay or sandstone. The third survey line was oriented from the west-northwest to the southeast, with coordinates 7°12’50.84” S, 112°46’35.68” E to 7°12’53.08” S, 112°46’40.38” E, as depicted in Figure 8(c). The resistivity values along this line ranged from 0.766 Ωm to over than 60.5 Ωm, with the layer interpreted as clay or standstone.

Based on the results from all three survey lines, it can be concluded that the subsurface layers at the second test location of the study area predominantly consist of clay or sandstone formations.

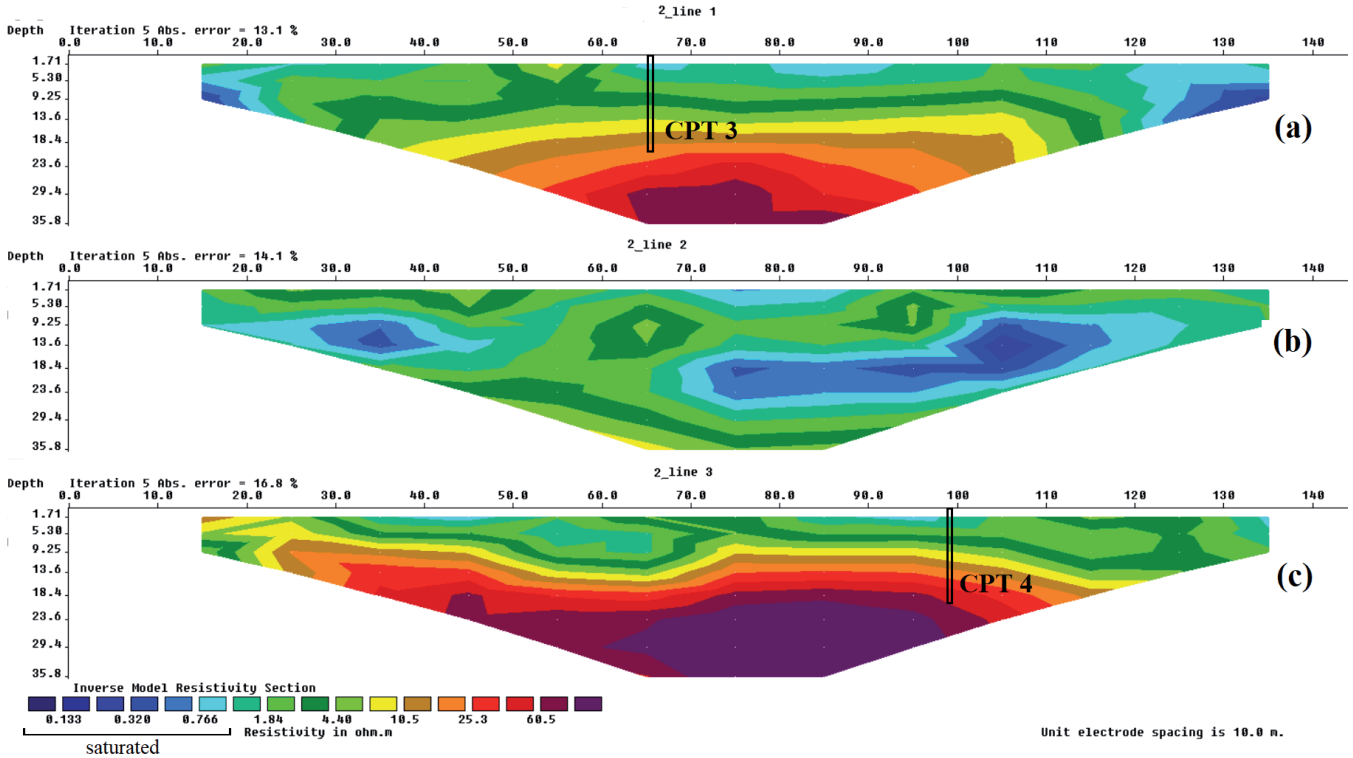

Figure 8 Two-dimensional cross-sectional representation of subsurface layers at the second site: (a) first profile, (b) second profile, and (c) third profile.

At the third test location, the trajectory of cable 1 was extended from the northwest to the southeast, with coordinates ranging from 7°12’25.63” S, 112°46’25.44” E to 7°12’28.50” S, 112°46’29.61” E. Figure 9 shows the map of the first test location.

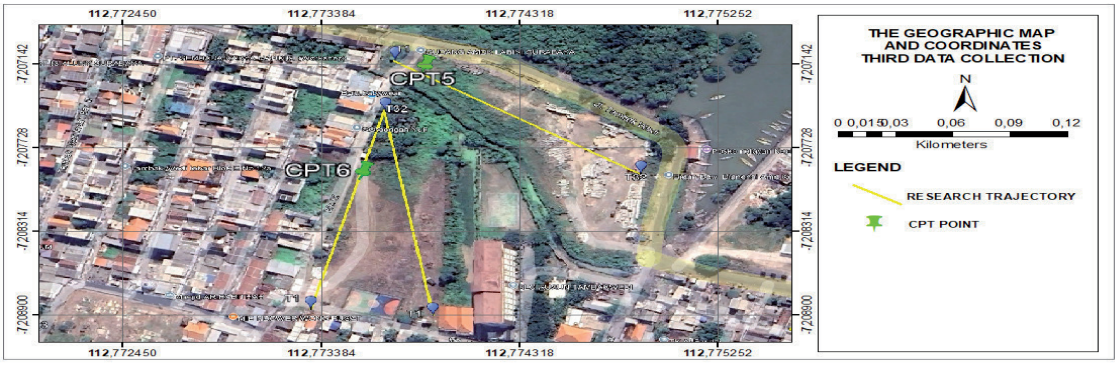

Figure 9 The geographic map and coordinates corresponding to the third data collection site.

A 2D subsurface profile was subsequently generated, as depicted in Figure 10(a). For the first trajectory, the resistivity values varied between 1.84 Ωm to over than 60.5 Ωm. Layers with resistivity values ranging from 1 Ωm to 100 Ωm were interpreted as clay or sandstone. The second trajectory as depicted in Figure 10(b), extending from the northeast to the southwest (coordinates 7°12'31.90" S, 112°46'24.02" E to 7°12'26.90" S, 112°46'25.27" E, yielded resistivity values from 0.319 Ωm to 4.39 Ωm, indicating the presence of clay or sandstone with an underlying seawater layer. The third trajectory as depicted in Figure 10(c), spanning from the north-northwest to the south-southeast (coordinates 7°12'32.06" S, 112°46'26.09" E to 7°12'26.90" S, 112°46'25.27" E), recorded resistivity values from 0.32 Ωm to 25.3 Ωm, suggesting a clay or a sandstone layer with seawater intrusion.

In conclusion, the subsurface at the third test location of the study area predominantly consists of clay or sandstone layers. However, the resistivity values indicate the presence of seawater intrusion, characterized by resistivity values below 1 Ωm.

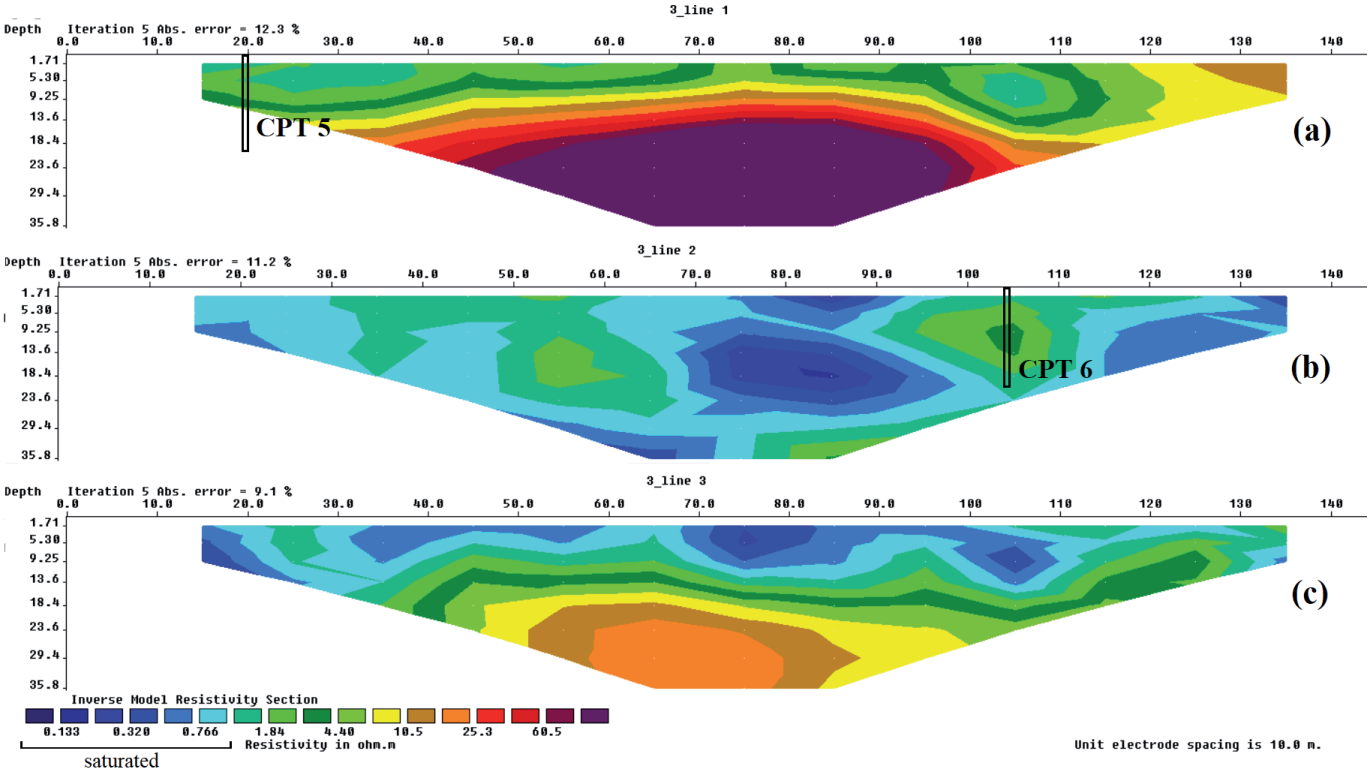

Figure 10 Two-dimensional cross-sectional representation of subsurface layers at the third site: (a) first profile, (b) second profile, and (c) third profile.

Analysis of Data Using the CPT

The CPT data was analyzed using Robertson's simplified method. The peak ground acceleration (PGA) for the test area is 0.3*g*, as referenced by the Indonesian Earthquake Map Revision Team (Irsyam et al., 2010). The seismic magnitude is assumed to be 7.5 Mw, given that Surabaya is situated above the Surabaya and Waru fault zones, both of which have

the potential to generate significant-magnitude earthquakes. The data analysis includes the computation of Standard Penetration Test (N-SPT) values to evaluate the liquefaction potential at the study site, employing the empirical correlation proposed by Danziger et al., (1998).

Data collection was conducted at a single point within the geoelectric survey. The distance between CPT points was maintained at a minimum of 50 meters, with each test reaching a depth of 20 meters. The potential for liquefaction is assessed based on the safety factor (SF) value. A SF value below 1 suggests a significant potential of liquefaction occurrence. The soil layer under investigation is characterized by a low q_c value and a high FR value. Typically, such a combination of a low q_c value and a high FR value is associated with a significant liquefaction potential. Furthermore, these relationships imply that, from a theoretical perspective, the soil layer is predominantly composed of silty clay.

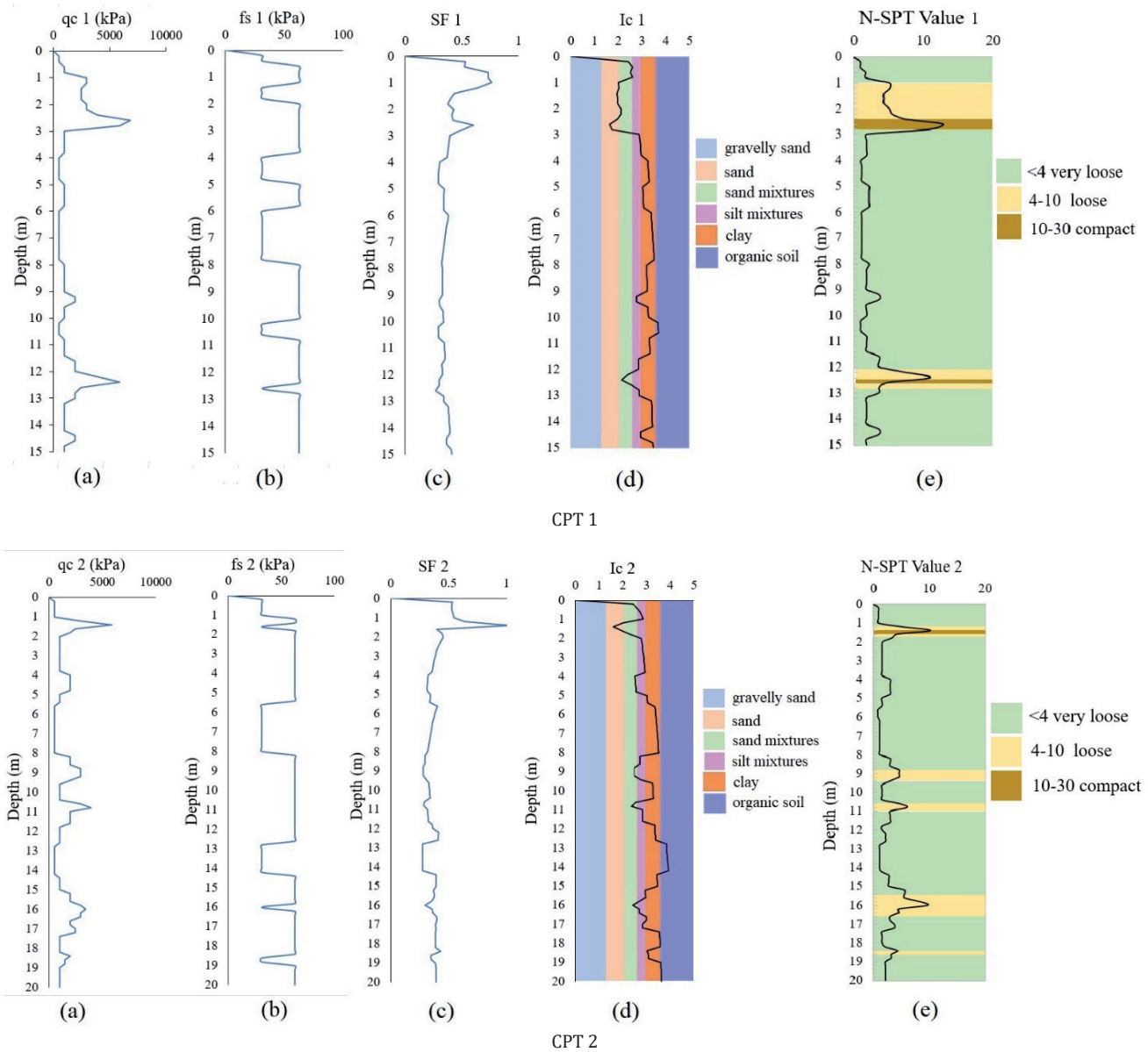

Figure 11. Liquefaction analysis at the first and the second CPT testing location, illustrating (a) q_c vs depth, (b) f_s vs depth, (c) safety factor (SF) vs depth, (d) soil behavior type index vs depth, and (e) N-SPT Value vs depth.

Analysis for CPT 1, in Figure 11(a), the values of q_c range from 490 to 6,864 kPa, while the f_s values range from 31.4 to 62.7 kPa as depicted in Figure 11(b). According to theoretical principles, a high q_c value coupled with a low f_s value indicates a potential for liquefaction in the study area. Data analysis using the simplified method reveals a safety factor (SF) of less than 1, as depicted in Figure 11(c). These results suggest that the test area exhibits a considerable potential for liquefaction. Furthermore, the soil stratigraphy can be determined

through the soil behavior type index, as shown in Figure 11(d). In the CPT 1 test location, the soil layers vary from sand to clay, with a predominance of clay layers observed between depths of 3 to 15 meters. The N-SPT data (Figure 11(e)) indicate that the subsurface profile is predominantly composed of very loose soils, interspersed with several loose layers and two dense soil layers. The dense layers are identified at depths of approximately 2.4 meters (with a thickness of 40 cm) and 12.6 meters (with a thickness of 20 cm), respectively.

Analysis for CPT 2, in Figure 10(a), the q_c ranges from 490 to 6,864 kPa, while the f_s varies between 31.4 and 62.7 kPa, as depicted in Figure 10(b). Upon performing a data analysis using the simplified method, the SF is found to be 1 at a depth of 1.5 meters. However, the SF decreases to below 1 between depths of 2 to 20 meters, as shown in Figure 10(c). These results suggest that the test area exhibits a significant potential for liquefaction. Furthermore, the type of soil layers can be identified through the soil behavior type index, as shown in Figure 10(d). In the CPT 2 test area, the soil composition varies from sand to organic soil, with a predominance of clay layers observed between depths of 5 to 20 meters. Based on the N-SPT values (Figure 9(e)), the soil profile is predominantly composed of very loose soil, with several loose layers and a single dense soil layer. The dense layer is located at a depth of 1.6 meters and has a thickness of 20 cm.

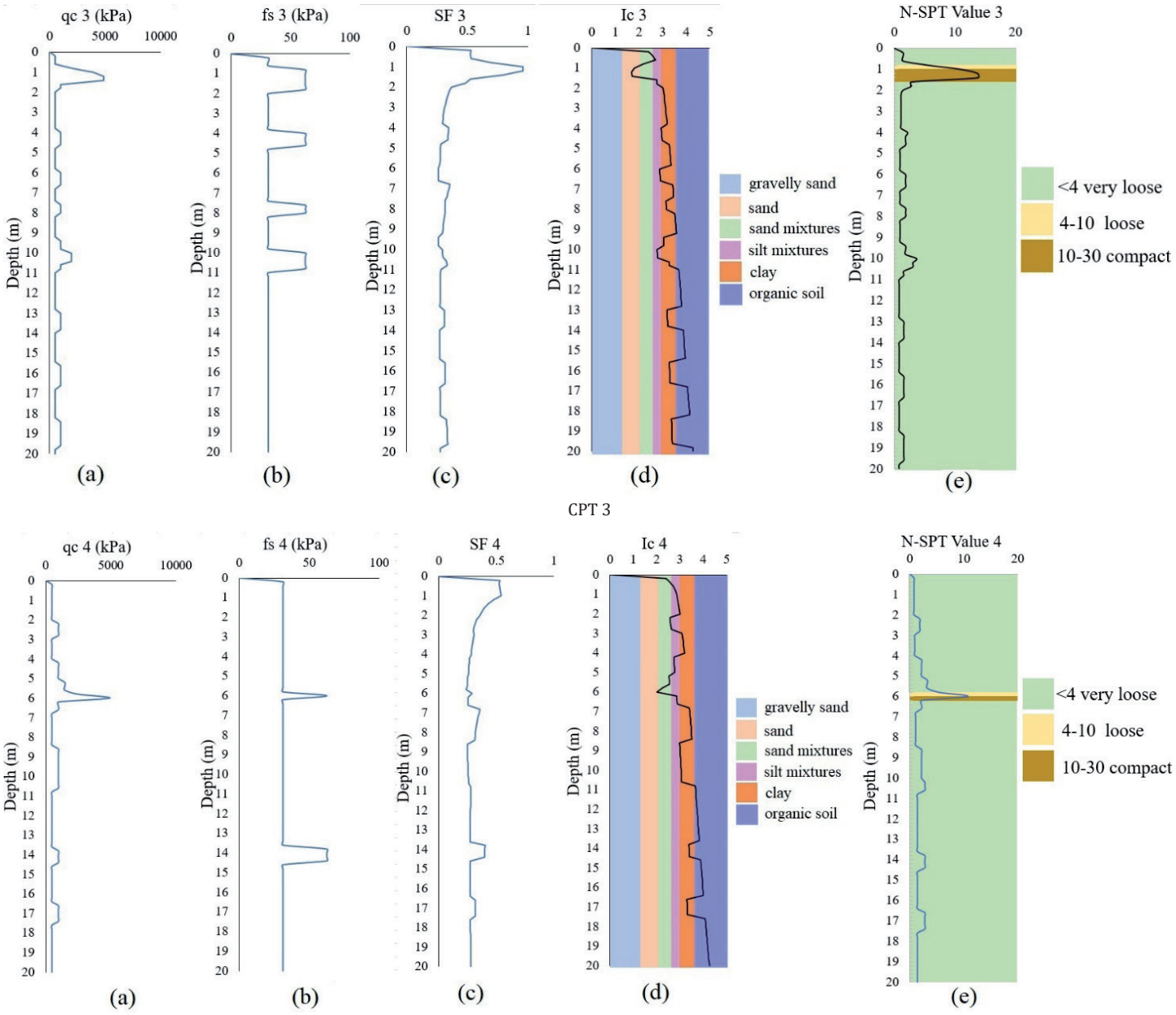

Figure 11. Liquefaction analysis at the third and the fourth CPT testing location, illustrating (a) q_c vs depth, (b) f_s vs depth, (c) safety factor (SF) vs depth, (d) soil behavior type index vs depth, and (e) N-SPT Value vs depth.

Analysis for CPT 3, in Figure 11(a), the q_c ranges still from 490 to 6,864 kPa, while the f_s varies between 31.4 and 62.7 kPa, as depicted in Figure 11(b). Upon performing a data analysis using the simplified method, the SF is found to be 1 at a depth of 1 meter, as illustrated in Figure 11(c). However, the SF decreases to below 1 between depths of 2 to 20 meters. These results suggest that the test area exhibits a considerable potential for liquefaction. Furthermore, the type of soil layers can be identified through the soil behavior type index, as shown in Figure 11(d). The soil composition varies from sand to organic soil, with a predominance of clay layers observed between depths of 2 to 19 meters and organic soil layers between depth 11 to 20 meters. Analysis of the N-SPT values presented in Figure 11(e) indicates that the soil at the CPT 3 testing site predominantly exhibits high susceptibility. This observation corroborates the elevated liquefaction potential inferred from the SF values. The dense layer is located at a depth of 1 meter and has a thickness of 60 cm.

Analysis for CPT 4, in Figure 11(a), the q_c ranges still from 490 to 6,864 kPa, while the f_s varies between 31.4 and 62.7 kPa, as depicted in figure 11(b). Upon performing a data analysis using the simplified method, the SF is found less than 1, as illustrated in Figure 11(c). These results suggest that the test area exhibits a significant potential for liquefaction. Furthermore, the type of soil layers can be identified through the soil behavior type index, as shown in Figure 11(d). In the CPT 4 test area, the soil composition varies from sand to organic soil, with a predominance of silt mixtures observed between depths of 1 – 7 meters and clay layers observed between depths of 2 to 17 meters. Analysis of the N-SPT values presented in Figure 11(e) indicates that the soil at the CPT 4 testing site predominantly exhibits high susceptibility. This observation corroborates the elevated liquefaction potential inferred from the SF values. The dense layer is located at a depth of 6 meters and has a thickness of 20 cm.

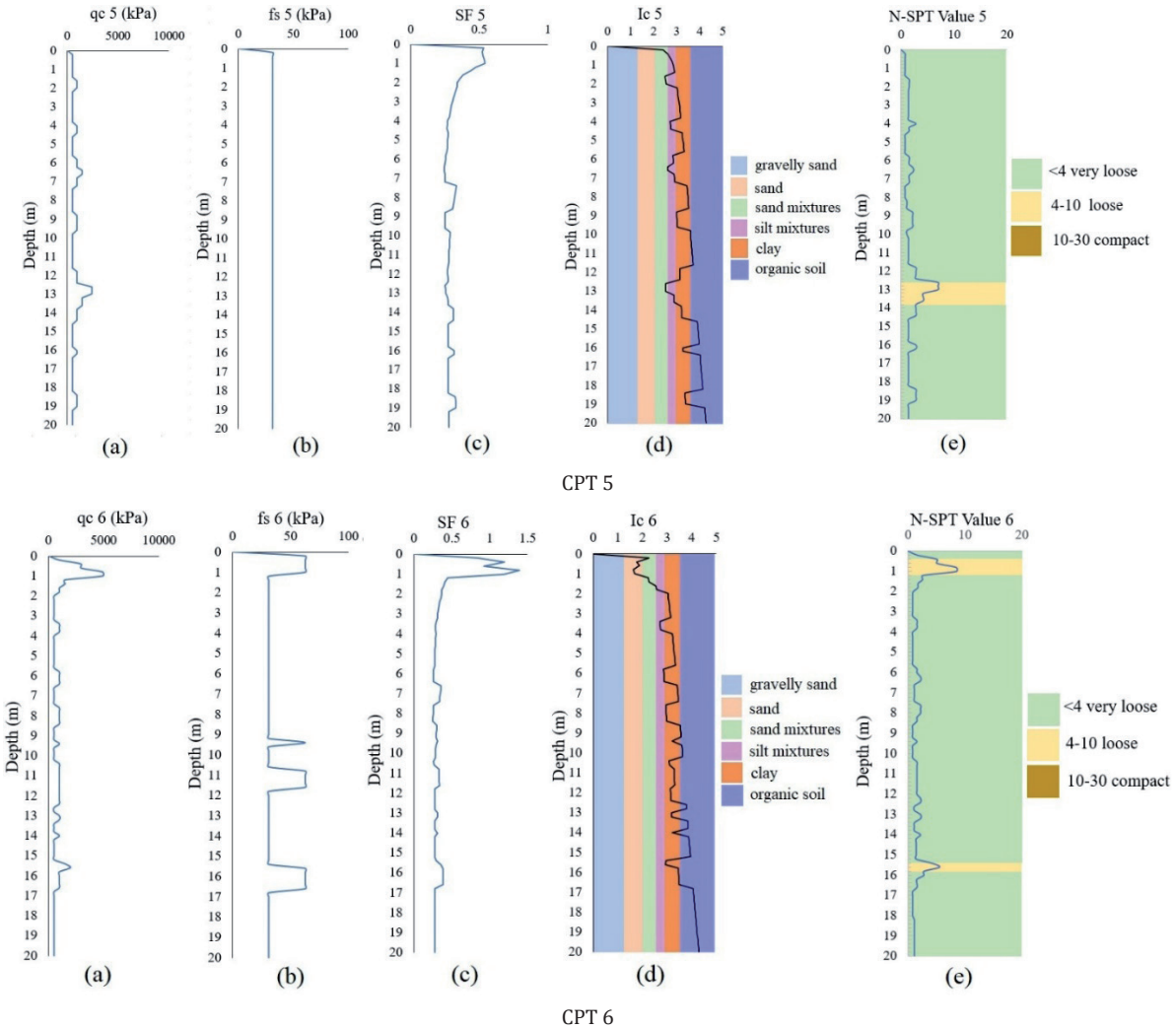

Figure 12. Liquefaction analysis at the sixth CPT testing location, illustrating (a) q_c vs depth, (b) f_s vs depth, (c) safety factor (SF) vs depth, (d) soil behavior type index vs depth, and (e) N-SPT Value vs depth.

Analysis for CPT 5, in Figure 12(a), the q_c ranges still from 490 to 6,864 kPa, while the f_s values constant at 31.2 kPa, as shown in Figure 12(b). Upon performing a data analysis using the simplified method, the SF is found less than 1, as illustrated in Figure 12(c). These results suggest that the test area exhibits a significant potential for liquefaction. Furthermore, the type of soil layers can be identified through the soil behavior type index, as shown in Figure 12(d). In the CPT 5 test area, the soil composition varies from sand mixtures to organic soil, with a predominance of clay layers observed between depths of 2 to 19 meters. Analysis of the N-SPT values presented in Figure 12(e) indicates that the soil at the CPT 5 testing site predominantly exhibits high susceptibility. This observation corroborates the elevated liquefaction potential inferred from the SF values. No compact soil layer was identified. However, loose soil layers were observed at a depth of 12.3 meters with a thickness of 120 cm.

Analysis for CPT 6, in Figure 12(a), the q_c ranges still from 490 to 6,864 kPa, while the f_s varies between 31.4 and 62.7 kPa, as shown in Figure 12(b). Upon performing a data analysis using the simplified method, the SF is found over than 1 at a depth of 1 meter. However, the SF decreases to below 1 between depths of 2 to 20 meters, as illustrated in Figure 12(c). These results suggest that the test area exhibits a significant potential for liquefaction. Furthermore, the type of soil layers can be identified through the soil behavior type index, as shown in Figure 12(d). In the CPT 6 test area, the soil composition varies from sand to organic soil, with a predominance of clay layers observed between depths of 2 to 17 meters. Analysis of the N-SPT values presented in Figure 12(e) indicates that the soil at the CPT 5 testing site predominantly exhibits high susceptibility. This observation corroborates the elevated liquefaction potential inferred from the SF values. No compact soil layer was identified. However, loose soil layers were observed at a depth of 0.4 meters with a thickness of 80 cm, and at a depth of 15.4 meters with a thickness of 40 cm.

5. Discussion

The Correlation Between Soil Resistivity Values and SF Values

In this study, the soil resistivity values obtained from the geoelectric resistivity method will be compared with the SF values derived from the CPT. The correlation between these two datasets will help assess whether both methods provide consistent interpretations of soil stratigraphy.

Table 5 The correlation between soil resistivity values and the SF values

Resistivity value (Ωm)	SF value
1.84	0.2 – 1.0
4.39 - 4.40	0.3 – 0.4
10.5	0.3 – 0.8
25.3	0.3 – 0.4
60.5	0.3

The analysis of resistivity and Safety Factor (SF) data in table 5 indicates that there is no strong linear correlation between the two variables. Although low resistivity values (less than 10 Ωm) generally align with low SF values, suggesting saturated and weak soils with high liquefaction potential, this trend becomes inconsistent at higher resistivity levels. Notably, a high resistivity value of 60.5 Ωm still corresponds to a low SF of 0.3, which contradicts the expectation that higher resistivity indicates more stable, less liquefiable soils. This inconsistency suggests that other factors such as soil density, grain structure, stratigraphy, and seismic loading play a significant role in determining SF, independently of resistivity. Therefore, while resistivity data can serve as a useful preliminary indicator of potential liquefaction zones, it cannot reliably predict liquefaction risk on its own. A comprehensive assessment must incorporate in-situ geotechnical data, particularly from Cone Penetration Tests (CPT), to accurately evaluate the soil's resistance to liquefaction.

Liquefaction Potential

Analysis of the N-SPT values presented in Figure 14(e) to 16 (e) indicates that the site predominantly exhibits high susceptibility. This observation corroborates the elevated liquefaction potential inferred from the SF values. Based on historical data compiled by several researchers, as presented in Table 6, the liquefaction triggering parameter values proposed by Cetin et al. (2004), Boulanger and Idriss (2014), and Sumartini (2021) were compared with the findings of the present study. Sumartini (2021) conducted cyclic triaxial testing on cohesive soils in the Kumamoto region of Japan. Despite the cohesive nature of the tested soils, the results demonstrated comparable liquefaction triggering parameter values to those reported in prior studies, indicating consistency across different soil types and research methodologies.

Table 6 Several data based on historical research.

Parameter	Cetin et al. (2004)	BI (2014) (SPT method)	**BI (2014) (CPT method)**	**Sumartini (2021) (Triaxial cyclic method)**	**Current Study**
"yes" cases	109	133	180	Yes	-
"No" cases	88	118	71	-	-
"yes/No" cases	3	3	2	-	-
Effective overburden stress (σ'_{vo})	8.1 – 198.7	20.3 – 170.9	19.0 – 147.0	60 and 90	3.34 – 163.63
N-SPT	2.2 – 66.1	4.6 – 63.7	16.1 – 311.9	5.8 – 6.8	0.8 – 12.8
CSR	0.05 – 0.66	0.04 – 0.69	0.06 – 0.65	0.5	0.3 – 0.4
Earthquake Magnitude	5.9 – 8.0	5.9 – 8.3	5.9 – 9.0	7	7.5

Referring to Table 6, liquefaction has been observed in soils with Standard Penetration Test (N-SPT) values ranging from 2.2 to 311.9. Based on this historical range, it can be inferred that the soil investigated in this study exhibits potential for liquefaction, as the measured N-SPT values (0.8–12.8) fall within this threshold. Although resistivity and Cone Penetration Test (CPT) results suggest that the subsurface material at the test site is likely cohesive, historical stratigraphic correlations indicate a high probability that the material is sandstone, as interpreted from resistivity data. Regardless of the classification, the potential for liquefaction remains present. This is supported by the findings of Sumartini (2021), who, through cyclic triaxial testing on type-2 cohesive volcanic soils under the standard Japanese Industrial Standards (JIS), demonstrated that cohesive soils may also undergo liquefaction when subjected to cyclic stress ratios (CSR) exceeding 0.5. A post-event investigation in Donggala, Palu following the 2018 liquefaction revealed that the N-SPT values in the affected zones were generally below 10 (Rohit et al., 2021). These findings provide a relevant point of comparison for evaluating the results of the current study.

The assessment of liquefaction potential can be further refined using the Liquefaction Potential Index (LPI) and the Liquefaction Severity Index (LSI). The LPI quantifies the susceptibility of a site to liquefaction, while the LSI provides an estimate of the potential damage severity resulting from liquefaction events. These indices offer complementary insights, particularly in field conditions where safety factor (SF) values are low, yet the subsurface profile is dominated by cohesive clay layers. The computed LPI and LSI values are summarized in Table 7.

Table 7 LPI and LSI value to determined the liquefaction risk.

No. CPT	**LSI**	**Severity of Liquefaction**	**LPI**	**Risk of Liquefaction**
1	116.61	Very high	9.54	Moderate
2	125.31	Very high	12.78	Moderate
3	129.61	Very high	13.55	Moderate
4	138.48	Very high	14.12	Moderate
5	139.25	Very high	14.20	Moderate
6	125.67	Very high	13.37	Moderate

6. Conclusions

This study demonstrates the efficacy of integrating geoelectrical resistivity measurements with Cone Penetration Test (CPT) data to evaluate subsurface liquefaction potential. The analysis identified a saturated zone extending from the surface to a depth of 35.8 meters, characterized by low resistivity (1.84–60.5 Ωm), low tip resistance (490–1,961 kPa), and low safety factor values (0.2–1.2), all of which are indicative of loosely packed, weakly consolidated soils prone to seismic-induced liquefaction.

Although a general correspondence was observed between low resistivity and low CPT-derived safety factors, the absence of a strong linear correlation underscores the influence of other geotechnical parameters. Moreover, Liquefaction Potential Index (LPI) and Liquefaction Severity Index (LSI) results reinforce the elevated hazard within the upper 35.8 meters of the profile, with LSI in particular pointing to a very high potential for structural damage.

These findings emphasize the importance of a multi-parameter assessment framework. Resistivity data provide valuable spatial insights into soil saturation and composition, while CPT testing yields critical mechanical and strength-related metrics. When used in combination, these methods significantly enhance the resolution and reliability of liquefaction risk evaluations. Nevertheless, additional in-situ or laboratory-based soil testing methods are required to validate and substantiate the findings of this study.

Acknowledgments

The author wishes to acknowledge the SAINTEK BRIN scholarship for its financial support of the master's program, the UB STARS program for providing research funding, the technicians and fellow students who contributed to the field data collection, the Head and colleagues at the Space Research Center for their encouragement in completing the research, and the colleagues at the Geological Disaster Research Center of BRIN for their insightful feedback during the preparation of this scientific article.

References

Ambarwati, I.W., Feranie, S., Tohari, A., 2020. Analisis Potensi Likuifaksi Pada Wilayah Cekungan Bandung Dengan Menggunakan Metode Uji Penetrasi Konus. Ris. Geol. Tambang 30, 21–32.

Atmakusuma, P.A., 2022. Memahami Likuifaksi: Analisa potensi, pemodelan dan pencegahannya untuk mewujudkan infrastruktur jalan yang andal dan berkelanjutan. Proc. Krtj 2022, 1–8.

Green, R.A., Ziotopoulou, K., 2015. Overview of screening criteria for liquefaction triggering susceptibility. Proc. 9th Pacific Conf. Earthq. Eng., 1–8.

Hardy, T., Nurdiyanto, B., Ngadmanto, D., Susilanto, P., 2015. Karakteristik Lapisan Tanah Berpotensi Likuifaksi Berdasarkan Resistivitas Batuan Di Daerah Cilacap. J. Meteorol. Geofis. 16, 45–53.

Hatmoko, J.T., Lulie, Y., 2008. Evaluasi potensi pencairan tanah (Liquefaction) akibat gempa, Studi kasus: Di bagian timur kota Yogyakarta. Konf. Nas. Tek. Sipil 2, 978–979.

Idriss, I.M., Boulanger, R.W., 2004. Evaluating the potential for liquefaction or cyclic failure of silts and clays. Center for Geotechnical Modeling, Univ. California, Davis.

Idriss, I.M., Boulanger, R.W., 2007. Soil liquefaction during earthquakes. Earthquake Engineering Research Institute, Oakland, CA.

Irsyam, M., Sengara, I.W., Aldiamar, F., Widiyantoro, S., Triyoso, W., Natawidjaja, D.H., Kertappati, E., Meilano, I., Suhardjono, Asrurifak, M., Ridwan, M., 2010. Ringkasan hasil studi tim revisi peta gempa Indonesia. Departemen Pekerjaan Umum, Jakarta.

Jarayanih, 2011. Geologi dan studi potensi likuifaksi daerah Srihandono dan sekitarnya, Kecamatan Pundong Kabupaten Bantul Propinsi Daerah Istimewa Yogyakarta. Thesis, Universitas Pembangunan Nasional Veteran, Yogyakarta.

Kavazanjian, E., Andrade, J.E., Arulmoli, K.A., Atwater, B.F., Christian, J.T., Green, R., Kramer, S.L., Mejia, L., Mitchell, J.K., Rathje, E., Rice, J.R., Wang, Y., Magsino, S., Gibbs, C.R., 2022. State of the Art and Practice in the Assessment of Earthquake-Induced Soil Liquefaction and Its Consequences. National Academies Press, Washington, DC.

Lowrie, W., 2007. Fundamentals of Geophysics, 2nd ed. Cambridge University Press, New York.

Mahmood, A.A., Mulligan, C.N., 2002. Liquefaction studies: A review. Proc. Annu. Conf. Can. Soc. Civ. Eng., 37–46.

Pratama, R.J.A., Krisnamurti, Wicaksono, L.A., 2022. Analysis of the liquefaction potential of palu city using qualitative and quantitative methods. J. Tek. Sipil 18, 140–151.

Prayitno, D.P., Artati, H.K., 2021. Analisis potensi likuifaksi berdasarkan distribusi ukuran butir tanah dan data cone penetration test (CPT). Media Komun. Tek. Sipil 27, 242–249.

Raharjo, A.N., 2019. Aplikasi metode geolistrik konfigurasi dipole-dipole untuk perencanaan pembuatan bangunan sipil di daerah kota Batu, kecamatan Ciomas, kabupaten Bogor, Jawa Barat. Thesis, UIN Syarif Hidayatullah, Jakarta.

Robertson, P.K., 1990. Soil classification using the cone penetration test. Can. Geotech. J. 27, 151–158.

Robertson, P.K., 2010. Soil behaviour type from the CPT: an update. Proc. 2nd Int. Symp. Cone Penetration Test., Huntington Beach, CA.

Robertson, P.K., Cabal, K.L., 2010. Estimating soil unit weight from CPT. Proc. 2nd Int. Symp. Cone Penetration Test., 1–8.

Robertson, P.K., Wride, C.E., 1998. Evaluating cyclic liquefaction potential using the cone penetration test. Can. Geotech. J. 35, 442–459.

Rohit, D., Hazarika, H., Maeda, T., Sumartini, W.O., Kokusho, T., Pasha, S.M.K., Nurdin, S., 2021. Forensic investigation on flowslides triggered by the 2018 Sulawesi earthquake. Prog. Earth Planet. Sci. 8, 60.

Santoso, D., 2007. Pengantar Teknik Geofisika. Penerbit ITB, Bandung.

Seed, H.B., Idriss, I.M., 1971. Simplified procedure for evaluating soil liquefaction potential. Report EERC 70-9, Univ. California, Berkeley.

Sonmez, H., Gokceoglu, C., 2005. A liquefaction severity index suggested for engineering practice. Environ. Geol. 48, 81–91.

Sumartini, W.O., 2021. Characteristics of Pumice and Their Influence on Earthquake-Induced Flow Failure in Gentle Slopes. Thesis, Kyushu University, Fukuoka.

Surabaya, P.K., 2016. Rencana pembangunan jangka menengah daerah (RPJMD) Kota Surabaya 2016 – 2021, Surabaya.

Susilo, A.J., Sumarli, I., Sentosa, G.S., Prihartiningsih, A., Wongkar, E., 2019. Effect of Compaction to Increase the Critical Height of a Slope without any Support. IOP Conf. Ser. Mater. Sci. Eng. 650, 012026.

Telford, W.M., Geldart, L.P., Sheriff, R.E., 1990. Applied Geophysics, 2nd ed. Cambridge University Press, Cambridge.

Wahyudi, H.D., Mutia, D., 2018. Interpretasi hasil uji penetrasi kerucut statis (Cone Penetration Test/CPT/Sondir) di Kawasan Bandar Udara Fatmawati Soekarno, Bengkulu. Agregat 3, 229–234.

Youd, T.L., Idriss, I.M., 2001. Liquefaction Resistance of Soils: Summary Report from the 1996 NCEER and 1998 NCEER/NSF Workshops on Evaluation of Liquefaction Resistance of Soils. J. Geotech. Geoenviron. Eng. 127, 297–313.